Letter

Correlation induced magnetic topological phases in the mixed-valence compound SmB_6

Huimei Liu,[1,2] Moritz M. Hirschmann,[2] George A. Sawatzky,[3,4] Giniyat Khaliullin,[2] and Andreas P. Schnyder[2]

[1]*Institute for Theoretical Solid State Physics and Würzburg-Dresden Cluster of Excellence ct.qmat, IFW Dresden, Helmholtzstr. 20, 01069 Dresden, Germany*

[2]*Max Planck Institute for Solid State Research, Heisenbergstrasse 1, D-70569 Stuttgart, Germany*

[3]*Department of Physics and Astronomy, University of British Columbia, Vancouver B.C. V6T 1Z1, Canada*

[4]*Stewart Blusson Quantum Matter Institute, University of British Columbia, Vancouver B.C. V6T 1Z4, Canada*

(Received 4 May 2023; revised 25 September 2023; accepted 7 November 2023; published 27 November 2023)

SmB_6 is a mixed-valence compound with flat f-electron bands that have a propensity to magnetism. Here, using a realistic Γ_8 quartet model, we investigate the dynamical spin susceptibility and describe the in-gap collective mode observed in neutron scattering experiments. We show that as the Sm valence increases with pressure, the magnetic correlations enhance and SmB_6 undergoes a first-order phase transition into a metallic antiferromagnetic state, whose symmetry depends on the model parameters. The magnetic orderings give rise to distinct band topologies: while the A-type order leads to an overlap between valence and conduction bands in the form of Dirac nodal lines, the G-type order has a negative indirect gap with weak $\mathbb{Z}_2$ indices. We also consider the spin polarized phase under a strong magnetic field, and find that it exhibits Weyl points as well as nodal lines close to the Fermi level. The magnetic phases show markedly different surface states and tunable bulk transport properties, with important implications for experiments. Our theory predicts that a magnetic order can be stabilized also by lifting the Γ_8 cubic symmetry, thus explaining the surface magnetism reported in SmB_6.

DOI: 10.1103/PhysRevResearch.5.L042028

Introduction. In the recent years, the fields of band topology [1] and heavy fermions [2] have intertwined to form the new research direction of topological heavy-fermion materials [3–13]. These materials exhibit topologically nontrivial band structures together with a number of strong-correlation effects, e.g., non-Fermi liquid behavior, unconventional quantum criticality, and Kondo lattice physics. The interplay between topology and electron correlations creates various novel phenomena, whose robust nature makes them amenable for topological quantum devices [14,15]. Correlation induced topological properties include exceptional points in quasiparticle spectra [9], giant spontaneous Hall effects [11], and helical magnetism induced by Weyl electrons [12]. Yet another intriguing possibility is that the magnetism of f electrons may alter the band topology of the charge carriers. This is what we study here in the context of the mixed-valence, heavy-fermion material SmB_6 [16–18].

The electronic structure of SmB_6 is characterized by strongly correlated $4f$ and itinerant $5d$ electrons, whose hybridization opens up a gap at the Fermi level with nontrivial topology [3,19,20]. The Sm valence fluctuates between Sm^{2+} and Sm^{3+} states. Its average value v can be tuned by pressure, in favor of magnetic Sm^{3+} with smaller ionic size, as sketched in Fig. 1(a). With increasing Sm valence, SmB_6 undergoes a discontinuous insulator-to-metal transition, accompanied by antiferromagnetic (AFM) order [21–26]. Remarkably, this transition occurs at an intermediate valence, $v_c \sim 2.7$ [24,25], well before reaching the fully trivalent state, such that valence fluctuations coexist with magnetism. This intriguing phase transition calls for a new theoretical description. In particular, the tunable interplay between band topology and magnetism at intermediate valence may give rise to new types of topological characteristics with interesting surface properties.

In this Letter, we address the above points based on a realistic model which reproduces the insulating band structure of SmB_6, as well as gives rise to a low-energy collective spin excitation below the charge gap, manifesting the proximity to magnetic order. In our theory, which explicitly includes the Sm valence v as a tuning parameter, the spin exciton softens and gains intensity as v increases. At a critical value of v_c, an insulator-to-magnetic-metal phase transition of first order takes place. The transition is driven by the exchange interactions between magnetoactive Sm^{3+} ions, whose density increases with pressure. Depending on the model parameters, different AFM states (such as A- or G-type orders) can form. We found that the magnetic phases exhibit band topologies that are markedly different from the insulating nonmagnetic phase. While the A-type order has nodal lines with surface states [27] at the Fermi level, the G-type order shows an indirect negative band gap with weak $\mathbb{Z}_2$ indices and corresponding Dirac surface states. In the spin polarized phase under a strong magnetic field, SmB_6 becomes a nodal-line Weyl semimetal. We characterize these band topologies by use of mirror Chern numbers, $\mathbb{Z}_2$ invariants, and a newly introduced "glide-mirror-graded" Wilson loop.

The model. The SmB_6 crystal has cubic symmetry, with B ions forming an octahedron at the cube center and Sm ions at

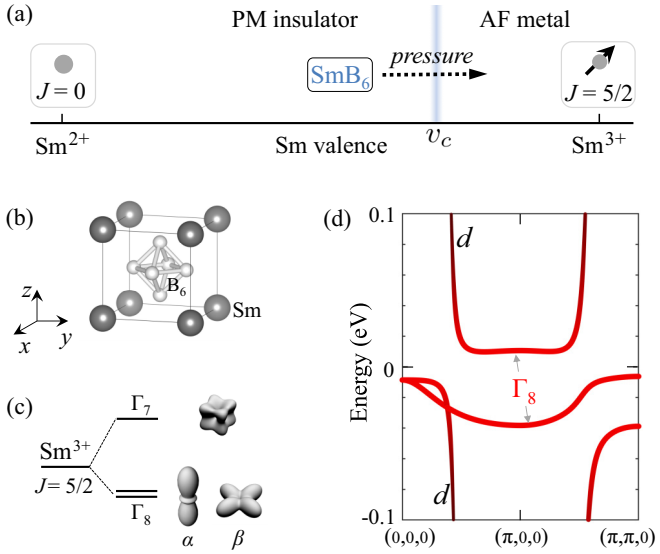

FIG. 1. (a) Sketch of the Sm ionic states and phase behavior of SmB_6 under pressure. (b) Lattice structure of SmB_6. (c) Crystal field splitting of the $J = 5/2$ multiplet into Γ_8 quartet and Γ_7 doublet. The Γ_8 quartet has a two-fold orbital degeneracy, α and β Kramers doublets with elongated and planar spatial shapes. (d) Low energy band structure of SmB_6 showing an insulating gap at the Fermi level. The black and red colors indicate the contributions from the highly dispersive $5d$ and quasilocalized $4f(\Gamma_8)$ states, respectively.

the cube corners, see Fig. 1(b). A hybridization of the Sm $4f$ orbitals with conduction bands leads to valence fluctuations between nearly degenerate $Sm^{2+}(f^6)$ and $Sm^{3+}(f^5)$ states. The resulting wavefunction can effectively be expressed as a coherent superposition $\sqrt{1-n}\,|f^6; d^0\rangle + \sqrt{n}\,|f^5; d^1\rangle$, where $|d\rangle$ denotes the Sm $5d$ band states admixed with B $2p$ orbitals, and $n = v - 2$ is the density of the magnetic Sm^{3+} ions.

The $Sm^{2+}(f^6)$ ion has a $J = 0$ singlet ground state. For Sm^{3+} with the f^5 configuration, the lowest multiplet is the $J = 5/2$ sextet, which is split by the cubic crystal field into a Γ_8 quartet and a Γ_7 doublet, see Fig. 1(c). In SmB_6, the Γ_7 level is about 20 meV higher in energy [28]. Moreover, the Γ_7 and $5d$ states have a negligible wavefunction overlap. Hence, we neglect the Γ_7 excitation, and focus on the Γ_8 quartet, the $J = 0$ singlet of Sm^{2+}, and the $5d$ bands to construct a low-energy Hamiltonian.

By symmetry, the transitions between $f^6(J = 0)$ and $f^5(J = 5/2; \Gamma_8)$ states can be described as the removal/addition of an f electron with the angular momentum $j = 5/2$ and Γ_8 symmetry. This mapping, which rescales the bare f-electron hopping amplitudes by the coefficients of fractional parentage [29], leads to the following Hamiltonian:

$$\begin{aligned}\mathcal{H} = {} & E_d \sum_{i\sigma\gamma} d^\dagger_{i\sigma\gamma} d_{i\sigma\gamma} + \sum_{ij}\sum_{\sigma\gamma\gamma'} t_{d,ij} d^\dagger_{i\sigma\gamma} d_{j\sigma\gamma'} \\ & + E_f \sum_{i\sigma\gamma} f^\dagger_{i\sigma\gamma} f_{i\sigma\gamma} + \sum_{ij}\sum_{\sigma\sigma'\gamma\gamma'} t_{f,ij} f^\dagger_{i\sigma\gamma} f_{j\sigma'\gamma'} \\ & + \sum_{ij}\sum_{\sigma\sigma'\gamma\gamma'} V_{ij} (d^\dagger_{i\sigma\gamma} f_{j\sigma'\gamma'} + \text{H.c.}), \end{aligned} \tag{1}$$

where $d^\dagger_{i\sigma\gamma}$ ($f^\dagger_{i\sigma\gamma}$) denote the creation operators of the $5d$ band (Γ_8 quartet) states on site i with (pseudo)spin σ and orbital index γ. The spin-orbital structure of the matrix elements t_d, t_f, and V follows from the symmetries of the $5d$ and $4f(\Gamma_8)$ wavefunctions [19,30] (see the Supplemental Material for details [31]). The Γ_8 quartet may be either fully occupied (Sm^{2+}) or host a single hole (Sm^{3+}). We treat this constraint on a mean-field level, and vary the energy levels E_d and E_f to control the f-hole density $n = v - 2$. The hopping amplitudes, renormalized by the correlation effects, are determined by a fit to experiments [31].

The band structure near the Fermi level, calculated at the valence $v = 2.56$ (i.e., at ambient pressure), is shown in Fig. 1(d). We observe two flat bands originating from the Γ_8 states, and one highly dispersive band of $5d$ character. Their hybridization opens up an insulating band gap of $\sim$17 meV, consistent with experiment [32]. The band inversion between the Γ_8 and d bands at the X point $(\pi, 0, 0)$ leads to a nontrivial strong $\mathbb{Z}_2$ topology with helical surface states [3,19,20].

Spin exciton and magnetic order. Having the model that reproduces the low-energy electronic states of SmB_6, we address now its magnetic properties. In SmB_6, a dispersive magnetic mode is formed inside the charge gap [33]. This is a signature of strong correlations among the $J = 5/2$ moments, which interact via the conduction bands or various superexchange channels (e.g., via the B orbitals). For simplicity, we model these interactions by the isotropic exchange Hamiltonian,

$$\mathcal{H}_{\text{ex}} = \sum_{\langle ij\rangle} \mathcal{J}_{ij} \boldsymbol{J}_i \cdot \boldsymbol{J}_j, \tag{2}$$

and calculate the dynamical magnetic susceptibility using the random phase approximation

$$\chi(\boldsymbol{q}, \omega) = \frac{\chi_0(\boldsymbol{q}, \omega)}{1 + \mathcal{J}_{\boldsymbol{q}} \chi_0(\boldsymbol{q}, \omega)}. \tag{3}$$

Here, $\mathcal{J}_{\boldsymbol{q}} = \sum_{\boldsymbol{R}} \mathcal{J}_{\boldsymbol{R}} e^{i\boldsymbol{q}\cdot\boldsymbol{R}}$ and $\chi_0(\boldsymbol{q}, \omega)$ is the bare magnetic susceptibility, which can readily be evaluated using the eigenstates and energies of the electronic bands obtained above [31]. The major contribution to $\chi_0(\boldsymbol{q}, \omega)$ is due to the transitions between the flat bands in Fig. 1(d), which give rise to a gapped Stoner continuum. Of our prime interest is, however, a low-energy collective mode that emerges as a sharp particle-hole bound state inside the gap [33–35]. From Eq. (3), the energy $\omega_{\boldsymbol{q}}$ of this mode is given by the condition $\mathcal{J}_{\boldsymbol{q}} = -1/\chi_0'(\boldsymbol{q}, \omega_{\boldsymbol{q}})$, and thus sensitive to the exchange parameters.

Having no microscopic theory for exchange interactions in SmB_6, we consider a minimal set of the $\mathcal{J}_{ij}$ couplings up to third-nearest neighbors. Figure 2(a) shows the spin-exciton peaks in $\chi''(\boldsymbol{q}, \omega)$, calculated using the parameter set $(\mathcal{J}_1, \mathcal{J}_2, \mathcal{J}_3) = (14.7, 6.5, 2.7)$ meV. The results for $v = 2.56$ qualitatively agree with the inelastic neutron scattering data [33].

We find that the spin exciton mode is highly sensitive to the valence state. It strongly softens and gains a large spectral weight as v increases, see Fig. 2(a). Physically, increasing the density of magnetic Sm^{3+} ions tips the balance between the exchange interactions and the f-electron delocalization

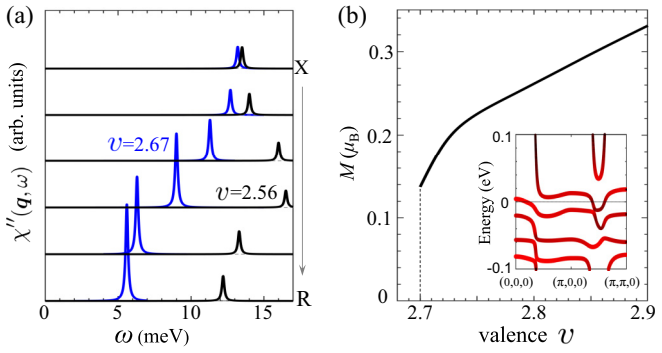

FIG. 2. (a) Dynamical magnetic susceptibility $\chi''(\boldsymbol{q},\omega)$ for the valence $\upsilon = 2.56$ (black) and 2.67 (blue), for $\boldsymbol{q}$ values along the high symmetry path from $X = (\pi, 0, 0)$ to $R = (\pi, \pi, \pi)$. The particle-hole continuum (not shown) is above $\simeq 17$ meV. (b) The G-type ordered magnetic moment M as a function of υ. The inset shows the metallic band structure at $\upsilon = 2.72$.

energy, driving the system toward a magnetic instability. SmB_6 develops a long-range AFM order at the critical valence $\upsilon_c \sim 2.7$ [24,25]. To describe this transition, we perform a mean-field calculation for the magnetic order parameter as a function of υ. We let the effective hopping parameters (t_d, t_f, V) vary as the valence increases under pressure, and rescale them by a phenomenological factor $[1 + \eta(\upsilon - \upsilon_0)]$, where $\upsilon_0 = 2.56$. Physically, the sign of the parameter η is determined by two competing effects: on the one hand, the effective hoppings are reduced ($\eta < 0$) by the correlations that enhance with valence υ; on the other hand, they increase ($\eta > 0$) due to the increased wavefunction overlap under pressure. With $\eta = 0.6$ [36], a magnetic solution appears at $\upsilon_c \simeq 2.7$ via a first-order phase transition, see Fig. 2(b). Once the magnetic order is established, the spin degeneracy is lifted and the band structure gets rearranged, which induces a simultaneous insulator-to-metal transition. The feedback effects between spin order and band structure result in a discontinuous transition, as observed in SmB_6 [21,23].

It should be noted that the AFM ordering pattern (not yet fully identified experimentally) is decided by the choice of $\mathcal{J}_{ij}$ parameters. While the above $\mathcal{J}_{ij}$ values (motivated by the spin-exciton dispersion fits) support G-type (Néel) state, other structures, such as A-type order suggested by a $(\pi, 0, 0)$ peak in the bare susceptibility $\chi_0(\boldsymbol{q})$ [31], are possible. Future experiments are required to quantify the exchange Hamiltonian in SmB_6.

Since the Γ_8 quartet is a spin-orbit entangled object, magnetic order also affects the orbital shape of the f-electron cloud and thus reduces cubic symmetry of the paramagnetic phase. Alternatively, lifting the degeneracy of the α and β states of the Γ_8 quartet [Fig. 1(c)] by uniaxial stress reduces the hybridization gap, thereby triggering magnetic order and an insulator-to-metal transition (Supplemental Material [31]); this is an interesting proposal for experiment. In fact, the Γ_8 quartet splitting is naturally present near the surface as well as near defects, and should be relevant for the analysis of the surface states and transport properties of SmB_6. For instance, the surface magnetism reported in SmB_6 [37,38] can

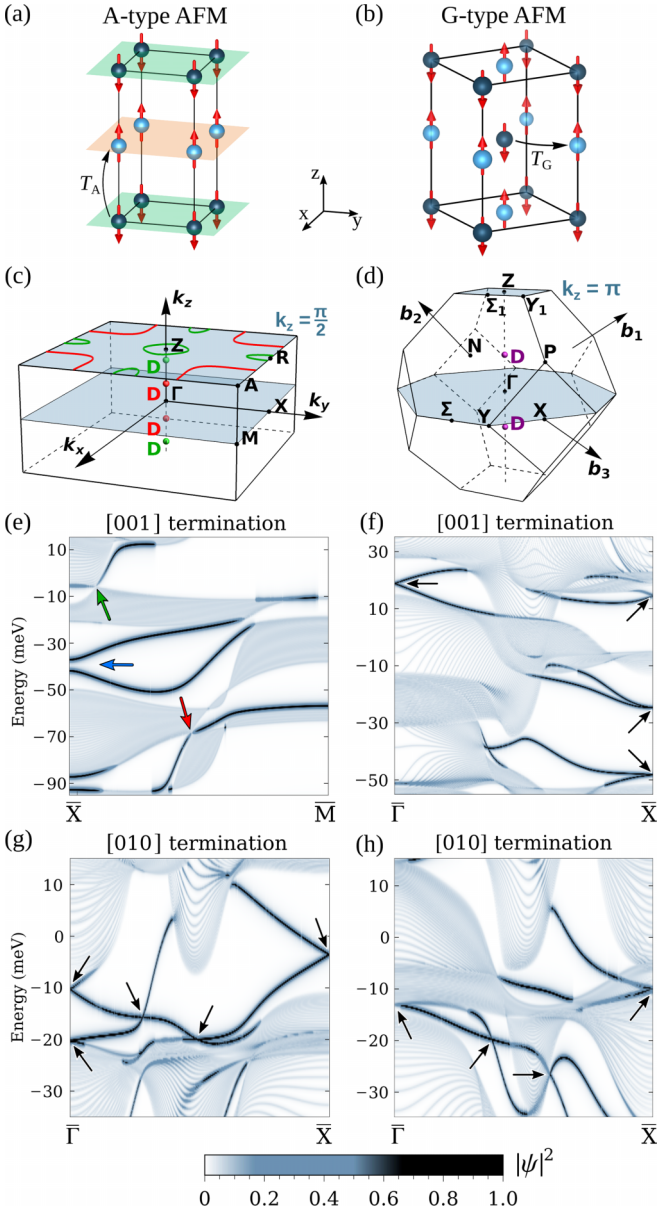

FIG. 3. Band topology of SmB_6 at valence $\upsilon = 2.74$ for the A-type (left) and G-type (right) antiferromagnetic states. (a), (b) Magnetic structures with moments indicated by the red arrows. (c), (d) Nodal lines and Dirac points in the vicinity (green) and below (red and purple) the Fermi level. (e)–(h) Band structures of a 100-layer slab with [001] and [010] termination, respectively. The color scale represents the wave function amplitude of the ten topmost layers. The arrows mark characteristic features of the different band topologies.

be understood as a natural consequence of the cubic symmetry breaking near the surface.

Topological properties. Paramagnetic SmB_6 is a topological insulator with strong and weak $\mathbb{Z}_2$ invariants and mirror Chern numbers [3]. Here, we present a topological analysis of the magnetically ordered metallic phases, based upon the Γ_8 quartet model of SmB_6. Specifically, we consider the two possible magnetic states, namely the A-type and G-type AFM orders shown in Figs. 3(a) and 3(b). Our topological analysis

is based on symmetries, and therefore applies also, at least qualitatively, to similar antiferromagnetic systems.

In the magnetic phases, the symmorphic symmetries $Pm\bar{3}m$ of the paramagnetic phase are lowered to nonsymmorphic magnetic space groups (MSG) [39]. For the A-type order we find the tetragonal MSG $P_{2c}4/mm'm'$, while for the G-type order the MSG is $P_I4/mm'm'$, which is body centered. Here we adopt the OG convention [39], for which the coordinate basis of the MSG coincides with the parent SG. Both MSGs contain magnetic translations, namely $T_A = T\,t(0,0,1)$ along the z axis for the A-type order and $T_G = T\,t(1,0,0)$ along the x axis for the G-type order, where $T = i\sigma_y K$ is the time-reversal operator. We note that T_G is equivalent to T_A up to a lattice vector of the G-type structure. Yet, the converse is not true, i.e., T_A is not equivalent to T_G up to a lattice vector of the A-type lattice.

To study the band topologies of the AFM phases, we compute the surface states and the associated topological numbers in our model, whereby we implement the coupling of the charge carriers to the AFM texture by an on-site Zeeman term. We find that for both AFM orders the bands are Kramers degenerate, due to the presence of both magnetic translations (T_A, T_G) and inversion (P) with $(PT_A)^2 = (PT_G)^2 = -1$. Moreover, both A- and G-type orders exhibit Dirac points below the Fermi level, while the A-type order has in addition nodal lines [31]. We now discuss these two AFM orders in more detail.

(i) The A-type order exhibits Dirac nodal lines in the $k_z = \frac{\pi}{2}$ plane for a large parameter range (due to the wide d band), see Fig. 3(c). These nodal lines are classified as type II [40], since they are strongly tilted. The appearance of Dirac nodal lines upon entering the A-type order defies the expectation that with less symmetries there are less symmetry-protected crossings. These Dirac nodal lines are protected by the m_z mirror symmetry together with PT_A. In the $k_z = \frac{\pi}{2}$ mirror plane PT_A pairs identical representations of m_z, such that two Kramers pairs with distinct m_z representations can cross in protected nodal lines. These nodal lines can be thought of as generalizations of lines protected by inversion and off-centered mirror symmetry [41,42].

By the bulk-boundary correspondence, one expects that these nodal lines lead to states localized on the [001] surface. Indeed, Fig. 3(e) shows nodal line surface states for the red and green nodal lines of Fig. 3(c), which however partially merge with bulk bands. In order to characterize the topology of these nodal lines and the associated surface states, one might consider a mirror Berry phase [27,43]. However, this quantity is unsuitable because the two orthogonal eigenspaces of the glide mirror symmetries $\tilde{m}_x$ and $\tilde{m}_y$ exchange along the k_z direction. Instead, we develop a "glide-mirror graded" Wilson loop [31]. The spectrum of this quantity, which resolves the band degeneracy caused by PT_A, exhibits a qualitative change at the nodal lines, i.e., the emergence of flat bands. Finally, on the [001] surface there appears also a gapped Dirac cone (blue arrow), which can be viewed as a remainder of the paramagnetic surface states, gapped by the magnetic order. While this is similar to an axion insulator [44,45], a half-integer Hall effect is not expected because of the gapless band structure.

On the [010] surface, on the other hand, there appear no nodal line surface states but only Dirac cones, indicated by black arrows in Fig. 3(g). These Dirac cones, found also in a band structure study [46] of the A-type order, are protected by mirror-Chern numbers and weak $\mathbb{Z}_2$ invariants defined within the $k_z = 0$ plane [31].

(ii) The G-type order does not have any nodal lines, but only Dirac cones on the Γ-Z axis protected by the fourfold rotation, see Fig. 3(d). Similar to the A-type order, the G-type order has weak $\mathbb{Z}_2$ invariants in two-dimensional subsystems where $T_G^2 = -1$ [1]. In particular, the three planes $k_x = 0$, $k_y = 0$, and $k_z = 0$, which each contain the time-reversal invariant momenta Γ, X, and Z, have nontrivial weak invariants [31]. By the bulk-boundary correspondence, these weak invariants lead to Dirac cone surface states for the [100], [010], and [001] terminations, see black arrows in Figs. 3(f) and 3(h).

Recent analysis of the quantum oscillation experiments at high magnetic fields suggested the presence of asymmetric nodal lines [47]. Motivated by this proposal, we consider the possibility of nodal lines in the high-field phase of SmB_6, where the moments are aligned ferromagnetically. In this state, any mirror plane may contain protected accidental nodal lines. Indeed, for the [001] alignment of the magnetic moments we find such nodal lines within the $k_z = 0$ and $k_z = \pi$ mirror planes, in close proximity to the Fermi level. These nodal lines are protected by a quantized π-Berry phase [31].

In conclusion, we have developed a theory for the insulator-to-magnetic-metal transition in SmB_6. We describe this transition as the softening of an in-gap spin exciton mode, which condenses into an AFM order at the critical density of magnetic Sm^{3+} ions. The AFM order induces a simultaneous insulator-to-metal transition as well as a change in the band topology. Within the Γ_8 quartet model, relevant to SmB_6, we find that the band structure is transformed from a cubic topological insulator to a tetragonal magnetic metal with symmetry protected Dirac points (G-type order) or Dirac points and nodal lines (A-type order). From our theory, we expect that the magnetic metal exhibits interesting transport characteristics, for example, light- or strain-induced anomalous Hall currents in the A-type order [48–50]. We hope that our findings will spur experimentalists to look for these intriguing properties, and to further characterize the insulator-to-magnetic-metal transition which can be induced in SmB_6 by pressure or uniaxial strain.

Acknowledgments. We thank Andreas Leonhardt for discussions. G.Kh. thanks the Max Planck-UBC-UTokyo Centre for Quantum Materials at the University of British Columbia, where this work was partially done, for hospitality. H.L. acknowledges support by the Würzburg-Dresden Cluster of Excellence on Complexity and Topology in Quantum Matter *ct.qmat* (EXC 2147, project ID 390858490). A.P.S. thanks the YITP Kyoto for hospitality.

H.L. and M.M.H. contributed equally to this work.

[1] C.-K. Chiu, J. C. Y. Teo, A. P. Schnyder, and S. Ryu, Classification of topological quantum matter with symmetries, Rev. Mod. Phys. **88**, 035005 (2016).

[2] S. Wirth and F. Steglich, Exploring heavy fermions from macroscopic to microscopic length scales, Nat. Rev. Mater. **1**, 16051 (2016).

[3] M. Dzero, K. Sun, V. Galitski, and P. Coleman, Topological Kondo insulators, Phys. Rev. Lett. **104**, 106408 (2010).

[4] P. P. Baruselli and M. Vojta, Scanning tunneling spectroscopy and surface quasiparticle interference in models for the strongly correlated topological insulators SmB_6 and PuB_6, Phys. Rev. B **90**, 201106(R) (2014).

[5] M. Sundermann, F. Strigari, T. Willers, H. Winkler, A. Prokofiev, J. M. Ablett, J.-P. Rueff, D. Schmitz, E. Weschke, M. M. Sala *et al.*, $CeRu_4Sn_6$: a strongly correlated material with nontrivial topology, Sci. Rep. **5**, 17937 (2015).

[6] P.-Y. Chang, O. Erten, and P. Coleman, Möbius Kondo insulators, Nat. Phys. **13**, 794 (2017).

[7] K. Kimura, T. Yoshida, and N. Kawakami, Topological properties of magnetically ordered heavy-fermion systems in the presence of mirror symmetry, J. Phys. Soc. Jpn. **87**, 084705 (2018).

[8] L. Li, K. Sun, C. Kurdak, and J. W. Allen, Emergent mystery in the Kondo insulator samarium hexaboride, Nat. Rev. Phys. **2**, 463 (2020).

[9] Y. Nagai, Y. Qi, H. Isobe, V. Kozii, and L. Fu, DMFT reveals the non-Hermitian topology and Fermi arcs in heavy-fermion systems, Phys. Rev. Lett. **125**, 227204 (2020).

[10] M. Klett, S. Ok, D. Riegler, P. Wölfle, R. Thomale, and T. Neupert, Topology and magnetism in the Kondo insulator phase diagram, Phys. Rev. B **101**, 161112(R) (2020).

[11] S. Dzsaber, X. Yan, M. Taupin, G. Eguchi, A. Prokofiev, T. Shiroka, P. Blaha, O. Rubel, S. E. Grefe, H.-H. Lai *et al.*, Giant spontaneous Hall effect in a nonmagnetic Weyl-Kondo semimetal, Proc. Natl. Acad. Sci. USA **118**, e2013386118 (2021).

[12] J. Gaudet, H.-Y. Yang, S. Baidya, B. Lu, G. Xu, Y. Zhao, J. A. Rodriguez-Rivera, C. M. Hoffmann, D. E. Graf, D. H. Torchinsky *et al.*, Weyl-mediated helical magnetism in NdAlSi, Nat. Mater. **20**, 1650 (2021).

[13] S. Wolgast, Y. S. Eo, T. Öztürk, G. Li, Z. Xiang, C. Tinsman, T. Asaba, B. Lawson, F. Yu, J. W. Allen *et al.*, Magnetotransport measurements of the surface states of samarium hexaboride using Corbino structures, Phys. Rev. B **92**, 115110 (2015).

[14] L. Šmejkal, Y. Mokrousov, B. Yan, and A. H. MacDonald, Topological antiferromagnetic spintronics, Nat. Phys. **14**, 242 (2018).

[15] M. J. Gilbert, Topological electronics, Commun. Phys. **4**, 70 (2021).

[16] A. Menth, E. Buehler, and T. H. Geballe, Magnetic and semiconducting properties of SmB_6, Phys. Rev. Lett. **22**, 295 (1969).

[17] C. M. Varma, Mixed-valence compounds, Rev. Mod. Phys. **48**, 219 (1976).

[18] P. F. S. Rosa and Z. Fisk, Bulk and Surface Properties of SmB_6, in *Rare-Earth Borides,* edited by D. S. Inosov (Jenny Stanford, New York, 2021).

[19] T. Takimoto, SmB_6: A promising candidate for a topological insulator, J. Phys. Soc. Jpn. **80**, 123710 (2011).

[20] F. Lu, J. Z. Zhao, H. Weng, Z. Fang, and X. Dai, Correlated topological insulators with mixed valence, Phys. Rev. Lett. **110**, 096401 (2013).

[21] A. Barla, J. Derr, J. P. Sanchez, B. Salce, G. Lapertot, B. P. Doyle, R. Rüffer, R. Lengsdorf, M. M. Abd-Elmeguid, and J. Flouquet, High-pressure ground state of SmB_6: electronic conduction and long range magnetic order, Phys. Rev. Lett. **94**, 166401 (2005).

[22] J. Derr, G. Knebel, G. Lapertot, B. Salce, M.-A. Méasson, and J. Flouquet, Valence and magnetic ordering in intermediate valence compounds: TmSe versus SmB_6, J. Phys.: Condens. Matter **18**, 2089 (2006).

[23] J. Derr, G. Knebel, D. Braithwaite, B. Salce, J. Flouquet, K. Flachbart, S. Gabáni, and N. Shitsevalova, From unconventional insulating behavior towards conventional magnetism in the intermediate-valence compound SmB_6, Phys. Rev. B **77**, 193107 (2008).

[24] N. P. Butch, J. Paglione, P. Chow, Y. M. Xiao, C. A. Marianetti, C. H. Booth, and J. R. Jeffries, Pressure-resistant intermediate valence in the Kondo insulator SmB_6, Phys. Rev. Lett. **116**, 156401 (2016).

[25] N. Emi, N. Kawamura, M. Mizumaki, T. Koyama, N. Ishimatsu, G. Pristáš, T. Kagayama, K. Shimizu, Y. Osanai, F. Iga *et al.*, Kondo-like behavior near the magnetic instability in SmB_6: Temperature and pressure dependences of the Sm valence, Phys. Rev. B **97**, 161116(R) (2018).

[26] Y. Zhou, Q. Wua, P. F. S. Rosa, R. Yu, J. Guo, W. Yi, S. Zhang, Z. Wang, H. Wang, S. Cai *et al.*, Quantum phase transition and destruction of Kondo effect in pressurized SmB_6, Sci. Bull. **62**, 1439 (2017).

[27] Y.-H. Chan, C.-K. Chiu, M. Y. Chou, and A. P. Schnyder, Ca_3P_2 and other topological semimetals with line nodes and drumhead surface states, Phys. Rev. B **93**, 205132 (2016).

[28] A. Amorese, O. Stockert, K. Kummer, N. B. Brookes, D.-J. Kim, Z. Fisk, M. W. Haverkort, P. Thalmeier, L. H. Tjeng, and A. Severing, Resonant inelastic x-ray scattering investigation of the crystal-field splitting of Sm^{3+} in SmB_6, Phys. Rev. B **100**, 241107(R) (2019).

[29] G. Sawatzky and R. Green, The explicit role of anion states in high-valence metal oxides, in *Quantum Materials: Experiments and Theory*, edited by E. Pavarini, E. Koch, J. van den Brink, and G. Sawatzky (Forschungszentrum Jülich, Jülich, 2016).

[30] K. Takegahara, Y. Aoki, and A. Yanase, Slater-Koster tables for f electrons, J. Phys. C: Solid State Phys. **13**, 583 (1980).

[31] See Supplemental Material at http://link.aps.org/supplemental/10.1103/PhysRevResearch.5.L042028 for details of the tight-binding model fits, the calculation of the magnetic susceptibility, the discussion of the mirror-graded Wilson loop, and the analysis of the band topology.

[32] M. Neupane, N. Alidoust, S.-Y. Xu, T. Kondo, Y. Ishida, D. J. Kim, C. Liu, I. Belopolski, Y. J. Jo, T.-R. Chang *et al.*, Surface electronic structure of the topological Kondo-insulator candidate correlated electron system SmB_6, Nat. Commun. **4**, 2991 (2013).

[33] W. T. Fuhrman, J. Leiner, P. Nikolić, G. E. Granroth, M. B. Stone, M. D. Lumsden, L. DeBeer-Schmitt, P. A. Alekseev, J.-M. Mignot, S. M. Koohpayeh *et al.*, Interaction driven subgap

spin exciton in the Kondo insulator SmB_6, Phys. Rev. Lett. **114**, 036401 (2015).

[34] P. S. Riseborough, Heavy fermion semiconductors, Ann. Phys. (Leipzig) **512**, 813 (2000).

[35] J. Knolle and N. R. Cooper, Excitons in topological Kondo insulators: theory of thermodynamic and transport anomalies in SmB_6, Phys. Rev. Lett. **118**, 096604 (2017).

[36] The value $\eta = 0.6$ leads to an increase of the hopping parameters by 8% at the critical pressure of $P \sim 6$ GPa, which sounds plausible.

[37] Y. Nakajima, P. Syers, X. Wang, R. Wang, and J. Paglione, One-dimensional edge state transport in a topological Kondo insulator, Nat. Phys. **12**, 213 (2016).

[38] A. Aishwarya, Z. Cai, A. Raghavan, M. Romanelli, X. Wang, X. Li, G. D. Gu, M. Hirsbrunner, T. Hughes, F. Liu, L. Jiao, and V. Madhavan, Spin-selective tunneling from nanowires of the candidate topological Kondo insulator SmB_6, Science **377**, 1218 (2022).

[39] S. V. Gallego, E. S. Tasci, G. Flor, J. M. Perez-Mato, and M. I. Aroyo, Magnetic symmetry in the bilbao crystallographic server: a computer program to provide systematic absences of magnetic neutron diffraction, J. Appl. Crystallogr. **45**, 1236 (2012).

[40] S. Li, Z.-M. Yu, Y. Liu, S. Guan, S.-S. Wang, X. Zhang, Y. Yao, and S. A. Yang, Type-II nodal loops: Theory and material realization, Phys. Rev. B **96**, 081106(R) (2017).

[41] B.-J. Yang, T. A. Bojesen, T. Morimoto, and A. Furusaki, Topological semimetals protected by off-centered symmetries in nonsymmorphic crystals, Phys. Rev. B **95**, 075135 (2017).

[42] J. Zhang, Y.-H. Chan, C.-K. Chiu, M. G. Vergniory, L. M. Schoop, and A. P. Schnyder, Topological band crossings in hexagonal materials, Phys. Rev. Mater. **2**, 074201 (2018).

[43] F. Zhang, C. L. Kane, and E. J. Mele, Topological mirror superconductivity, Phys. Rev. Lett. **111**, 056403 (2013).

[44] R. S. K. Mong, A. M. Essin, and J. E. Moore, Antiferromagnetic topological insulators, Phys. Rev. B **81**, 245209 (2010).

[45] C. Liu, Y. Wang, H. Li, Y. Wu, Y. Li, J. Li, K. He, Y. Xu, J. Zhang, and Y. Wang, Robust axion insulator and Chern insulator phases in a two-dimensional antiferromagnetic topological insulator, Nat. Mater. **19**, 522 (2020).

[46] K.-W. Chang and P.-J. Chen, Anomalous Z_2 antiferromagnetic topological phase in pressurized SmB_6, Phys. Rev. B **97**, 195145 (2018).

[47] N. Harrison, Highly asymmetric nodal semimetal in bulk SmB_6, Phys. Rev. Lett. **121**, 026602 (2018).

[48] W. B. Rui, Y. X. Zhao, and A. P. Schnyder, Topological transport in Dirac nodal-line semimetals, Phys. Rev. B **97**, 161113(R) (2018).

[49] T. Matsushita, S. Fujimoto, and A. P. Schnyder, Topological piezoelectric effect and parity anomaly in nodal line semimetals, Phys. Rev. Res. **2**, 043311 (2020).

[50] T. Oka and H. Aoki, Photovoltaic Hall effect in graphene, Phys. Rev. B **79**, 081406(R) (2009).